

Theoretical Studies of the Electronic and Thermoelectric Properties of PrIn_3 and NdIn_3 in Cubic Phase

Aiddah Naz¹, Qasimullah¹, Banaras Khan¹

¹Faculty of Physical and Numerical Sciences. Qurtuba University of Science and Information Technology, Peshawar 25100, Pakistan

qasimullah9966@gmail.com

September 25, 2024

Abstract

The electronic and thermoelectric properties of AB_3 (A = Pr, Nd and B = In) materials (crystallizing in the cubic structure) having space group Pm-3m (221) are studied using B3PW91 hybrid functional through the Full-Potential Linear Augmented Plane Wave (FP-LAPW) approach within the framework of Density Functional Theory (DFT). The calculated lattice parameters for PrIn_3 and NdIn_3 are 4.5668 Å and 4.5539 Å respectively. Electron-electron correlation effect is due to the 4f orbitals present in these materials and therefore, with the use of B3PW91 hybrid functional, band structure and density of states are calculated. When analyzing electron charge density, these materials showed a stronger ionic character. Band structure and density of state analysis confirms the metallic nature of the materials. Using the semi-empirical Boltzmann approach implemented in the BoltzTraP code, the thermoelectric parameters, such as Seebeck coefficient, figure of merit, electrical conductivity per relaxation time, and electronic thermal conductivity per relaxation time as a function of chemical potential, were computed at 500 K temperature gradient. PrIn_3 showed highest Seebeck coefficient value, $50.68 \mu\text{V} \div \text{K}$ among these compounds. The peak value of electrical conductivity per relaxation time and electronic thermal conductivity per relaxation time among these compounds is calculated for NdIn_3 is $2.43 \times 10^{20} \text{ 1}/\Omega\text{ms}$ and $22.50 \times 10^{14} \text{ W/mKs}$.

1 Introduction

Rare earth intermetallics play a distinctive role in a variety of technological applications, particularly in the realm of permanent magnets, and this is true from both a theoretical and practical perspective. These materials are identified to have heavy fermions, valence fluctuations, Kondo lattices, permanent-magnet materials, spin glasses, and random anisotropy systems. It is pointed out that in this vast number of materials there is an ideal chance of establishing which of several second-order terms are effective in determining structural stability. Dealing with intermetallic, the rare earths (RE) based intermetallics have promising of cubic crystal structure more favorable for industrial applications. [1-3]. The general chemical formula of the binary intermetallic compounds is AB_3 where A = Pr, Nd and B = In. The materials have space group Pm-3m No 221 and atomic position A is at (0, 0, 0), and B is located at $(0, \frac{1}{2}, \frac{1}{2})$ [4]. Schottky anomalies have been observed and analyzed in specific heat measurements on CeIn_3 , PrIn_3 . Susceptibility studies have led to the determination of the ground state levels in praseodymium compounds [5]. Diepen *et al.* [6] investigated heat capacities of AB_3 (A = Pr, Nd and B = In) systems which have been found between 7 and 300 K. The LaIn_3 calculations is adjust in a Debye curve of $\theta = 170 \text{ K}$. The magnetic properties of the AB_3 (A = Pr, Nd and B = In) compounds has been experimentally studied in the recent past comparing LaIn_3 to the other LnIn_3 compounds, LaIn_3 has a lower electronic specific heat coefficient ($5.3 \text{ mJ}/(\text{K}^2.\text{mol})$) and a higher gamma value ($120 \text{ mJ}/(\text{K}^2.\text{mol})$) than the other LnIn_3 compounds. SmSn_3 , EuSn_3 , and GdSn_3 exhibit

AFM transitions for the LnSn₃ series at temperatures $T_N = 12$ K, 36.5 K, and 16.5 K, respectively, based on magnetic susceptibility tests, where it was found that the majority of the lanthanide LnIn₃ compounds are AFM at low temperatures Sanchez *et al.* [7]. Onuki and Settai used Mössbauer resonance to determine the electrical and magnetic qualities of LnSn₃ compounds (Ln = La, Ce, Pr, Nd, Sm, Eu, Gd, Yb) [8]. The heat capacities were studied between 7 K and 300 K in a calorimeter of the adiabatic type [9]. With the exception of EuSn₃ and YbSn₃, LnIn₃ (Ln = Sn) exhibits the typical lanthanide contraction over the era induced by the insertion of another electron into the 4f orbital. The atom shrinks in size compared to its earlier iteration as a result of the increased nuclear charge's stronger attractive effect on the electron cloud. Because europium and ytterbium atoms are in a divalent (2+) and the other are in a trivalent (3+) ionic state, the lattice parameters of EuIn₃ and YbIn₃ are larger [10]. The Fermi surface of PrIn₃ is almost the same as that of the non-f reference material, LaIn₃. The Fermi surfaces and cyclotron masses of PrIn₃ are in the range of 0.3 m_0 to 1 m_0 , which are twice larger than those of LaIn₃ [11]. Magnetoresistance and de Haas-van Alphen (dHvA) effect in both the antiferromagnetic and paramagnetic states of NdIn₃ measured. Many dHvA branches are detected in the dHvA experiments. Among them, a nearly spherical Fermi surface in the paramagnetic state, which corresponds to a band 7-electron Fermi surface of the non-4f reference compound LaIn₃, is changed in the antiferromagnetic state into a multiply connected Fermi surface with necks. The cyclotron masses of NdIn₃ are in the range of 0.30 m_0 to 1.05 m_0 , which are twice as large as those of LaIn₃ [12]. The specific heats of RIn₃ (R = La, Ce, Pr, Nd, Sm, Gd, Tb and Ho) is measured between 0.2 and 2.2 K. The electronic specific heat coefficients are found to be enhanced for magnetic RIn₃ [13]. CeIn₃ possesses a large electronic specific heat coefficient ~ 130 mJ/K² mol at low temperature, indicating a heavy-electron system. Recently, the dHvA effect of PrIn₃, NdIn₃, SmIn₃, LaIn₃, CeIn₃ and GdIn₃ are measured. From the results of our dHvA experiments and band calculations done by Hasegawa *et al.* [14].

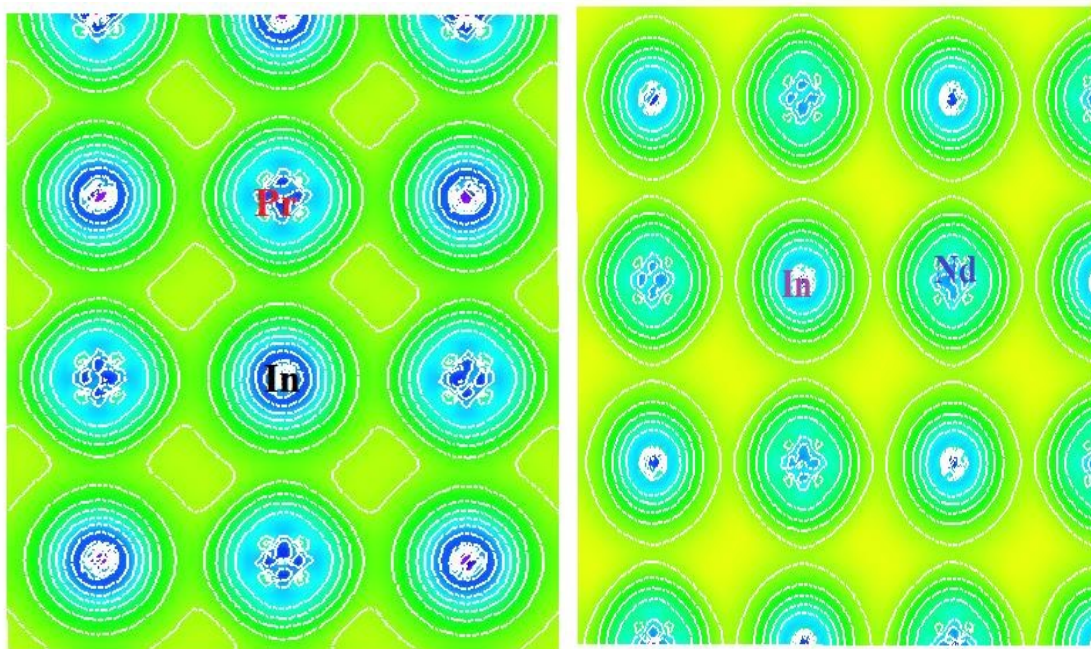
2 Method of Calculations

The bonding in these systems may be properly described by quantum mechanical methods. Nevertheless, current computing resources cannot resolve problems involving systems with more than a few atoms, making correct answers hard to get. Using approximate theoretical approaches, such as first principle or semi-empirical computations, is one method that can help us tackle these issues. First principles, also known as ab initio, are theoretical frameworks that begin with the proven fundamental laws of physics and do not rely on or make any presumptions, such as empirical models and parameter fitting. They don't rely on or make any assumptions. Using these methods is intended to get a clear description of the system's electronics wave function. The electrical structure of matter is studied using Density functional theory (DFT), a quantum mechanical modelling technique. Instead of utilizing the many-body wave function to describe the features of the many-body system, this DFT uses the functional rely on electron density of the system [15]. DFT has emerged as a potent theoretical tool to study the chemical and physical properties of crystal materials throughout the past century. On DFT, several researchers have worked. Over the past 20 years, it has been a commonly used instrument in the majority of chemical and material science domains. Because of its precision and low computing cost, DFT has gained popularity [16]. The density functional theory (DFT) framework, in combination with the full-potential Linearized Augmented Plane Wave (FP-LAPW) method, has been implemented using the WIEN2k package [17], to examine the electronic nature of PrIn₃ and NdIn₃. In order to determine the structural features, the local density approximation (LDA) was used to represent the exchange-correlation energy [18] and the generalized gradient approximation of Perdew *et al.* [19]. A straightforward method for enhancing calculations of numerous molecular parameters, including as optimization energies, bond lengths, and vibration frequencies, which frequently suffer from poor description by straightforward ab initio functionals, is hybridization with Hartree-Fock (HF) exchange, also known as exact exchange. The Hartree-Fock exact exchange functional and any number of exchange and correlation explicit density functionals are often linearly combined to create a hybrid exchange- correlation functional. The hybrid functionals implemented in wien2k are classified in to two types: full hybrid functionals and onsite hybrid functionals. For solid the full hybrid functional is computationally very expensive. On-site method as cheap as LDA/GGA. B3PW91 hybrid functionals are used to investigate the band structure and DOS for metallic materials [20]. The thermoelectric coefficients were determined by solving the Boltzmann transport properties using a constant relaxation time, the rigid band approximation, and first-principles calculations [21].

3 Results and Discussion

3.1 Electronic Charge Density

The electron charge density provides a thorough analysis of the bonding factor in the material and a significant representation of the majority of bonding. Similar to DFT, we deal with the material properties and identify the cell structure in order to estimate the electron charge density. The electron charge density is an analysis tool that can be used to better understand the structure of a material and how its atoms are bonded. This is achieved by looking at the distribution of electrons among individual atoms, which can determine whether bonding is covalent or ionic in nature. By understanding this relationship, scientists can gain a clearer view of the bulk bonding within a compound [22]. Researchers can quantify the spacing between the ions in the lattice and distinguish between different ions using data taken from the electron density plots. Researchers can quantify the spacing between the ions in the lattice and distinguish between different ions using data taken from the electron density graphs. Figures 3. 1 clearly show the present of ionic bonds which is present in all atoms. Nd makes strong ionic bond with In atom, because Nd electronegativity is higher than Pr.

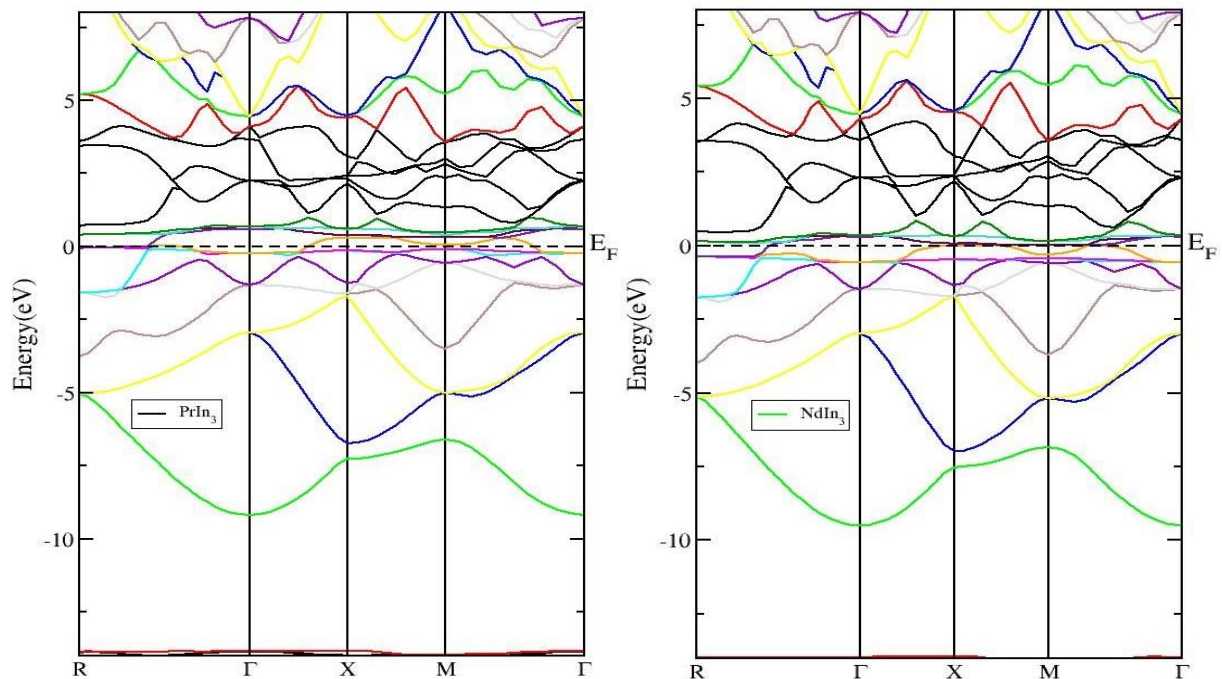


Figures 3.1 The electronic charge density of PrIn_3 and NdIn_3

3.2 Band Structure

One of the most fundamental parameters that defines a compound which has many physical properties would be its band gap. The band gap of a material is responsible for a complete measurement of different physical properties like optical, mechanical, optoelectronic and thermoelectric of the material. Because, the information of the electronic band structure of a material is important for its future technical implementation in various devices [23]. Electronic structure of a material plays an important role in determining their physical properties, particularly, the thermoelectric properties. The methods of determining electronic structure have developed swiftly during the last quarter of the twentieth century, particularly by the Density functional theory (DFT), due to the development of computer skills and the computation power. There are great numbers of DFT-based computational programs which can be accurately used to compute electronic structure of materials. Self-consistent field (SCF) computations are performed for the study of electronic band structures of these compounds as described earlier [24-26]. Exact value of the band gap and its nature

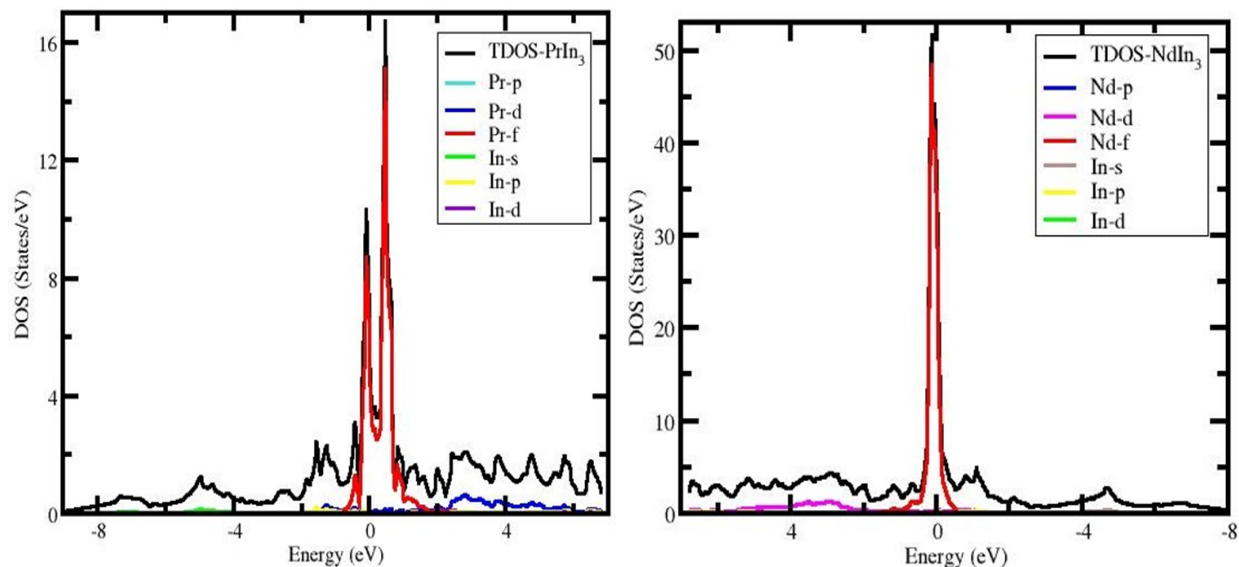
could be inferred from the band structure. The negative energy states correspond the valance band while the positive energy states correspond to the conduction band and E_f represent the Fermi energy level that coincide with the valance band edge at the zero energy states. In Figures 3.2 the energy range from -14 eV to 8 eV which is observed along the high symmetry directions in the first Brillouin zone. At zero pressure, the bands at the Fermi level for materials PrIn₃ and NdIn₃ are extremely similar along all high symmetry lines. The different colors in the band structure represent the energy states. Which is clearly described in DOS. At 0.0 eV, the Fermi energy level between the valance band and conduction band is assumed. The Figures 3.2 also show that in all compounds, the symmetry point R, τ , X and M is where the states overlap. No bandgap is observed for these compounds, hence all of them are metallic. The present study about PrIn₃ and NdIn₃ intermetallic materials show that there is no band gap between conduction and valance band make these compounds favorable for attaining novel materials properties.



Figures 3.2 The band structure of PrIn₃ and NdIn₃

3.3 Density of States

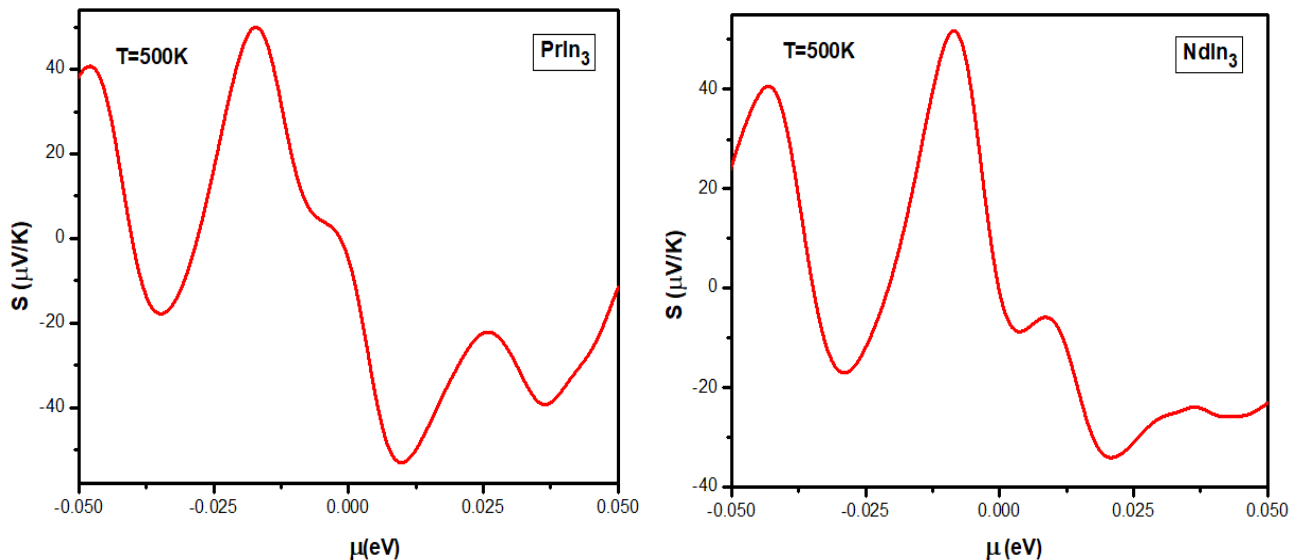
The density of states (DOS) of a system in solid state and condensed matter physics explains the number of states per energy per volume that will be filled by the system for each level of energy. The curves of density of states explained the contribution to the structure of the bands and the existence of the bonds. Band structure and the type of bonds are both explained by density of states. Figures 3.3 displays the total density of states (TDOS) as well as the partial density of states (DOS) for PrIn₃ and NdIn₃ materials. The density of states plots is shown in the Figures 3.3, where the negative energy states corresponds to the valance band while the positive energy states correspond to the conduction band and E_f represent the Fermi energy level that coincide with the valance band edge at the zero energy states. Figures 3.3 displays the results of the TDOS and PDOS computations for the PrIn₃ and NdIn₃ materials. The valance band and conduction band are mainly contributed by Pr/Nd and In for these materials. From the total density of states plots in Figure 3.3 one can't determine which states of Pr/Nd and In are contributing towards the conduction and valance band edges, this information is obtained from the plots of partial density of states given in Figures 3.3 which allow us to learn how frequently each state occurs in atoms conduction band and valance band. Pr-f, Pr-d, Nd-f and Nd-d make up the majority of the contribution at the Fermi level E_f and specifies the contribution and bonding at the Fermi level. The associated bonding is with the states In-s at the E_f , while rest of the states have negligible contribution.



Figures 3.3 The density of states of PrIn_3 and NdIn_3

3.4 Seebeck Coefficient

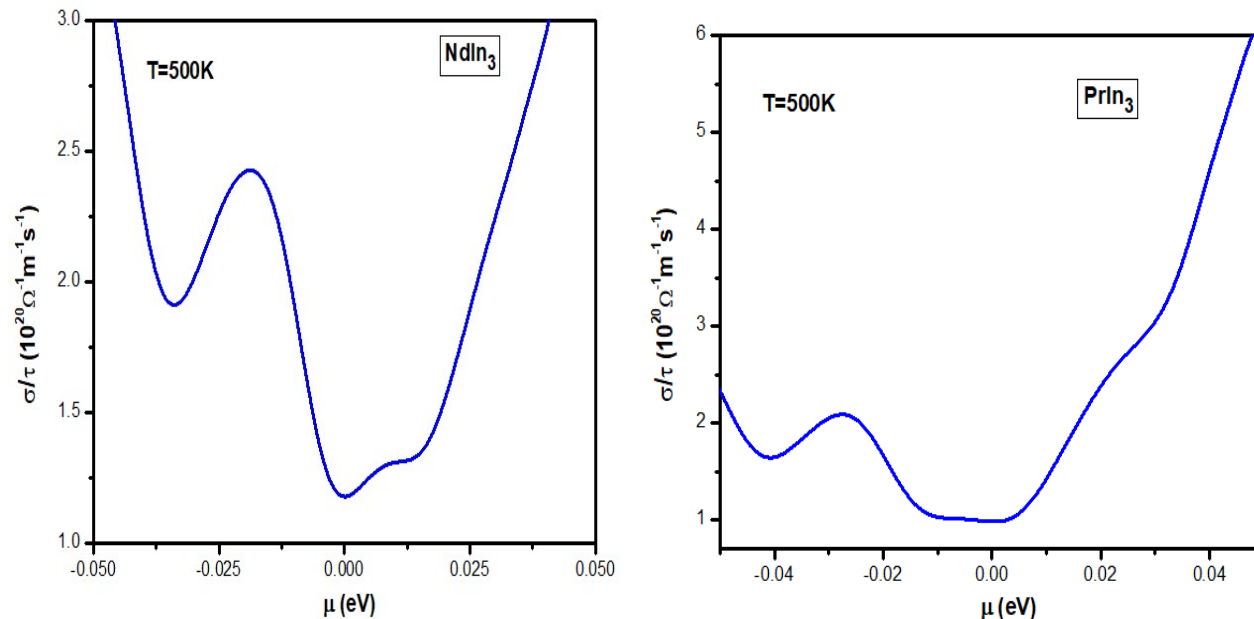
The Seebeck effect allows creation of voltage on the basis of the temperature difference. The magnitude of the effect is represented by the Seebeck parameter, S , given by the equation $S = V \div \Delta T$ where V is Voltage and ΔT is Temperature difference. When two different conductors are kept at different temperatures, the electrons on the hot end have high thermal energy than the electrons on the cold end. Therefore, electrons will flow towards the colder end. This net accumulation of electrons at the colder end gives a potential difference across the conductor, with the cold end being the negative. The materials with high Seebeck coefficient will have high Figure of merit that means greater capability to convert waste heat into useful electrical energy [27]. Different parameters are used to understand the thermoelectric phenomena. The most fundamental among these parameters is Seebeck coefficient which tells about the response of material to the applied temperature gradient. The value of Seebeck coefficient is negative for n-doped and is positive for p-doped. Chemical potential is defined as the concentration of the charge carrier in a material is the doping level of material. Chemical potential is important factor for enhancing thermoelectric nature. The plot of Seebeck coefficient against chemical potential for rare-earth intermetallic compounds AB_3 ($A=\text{Pr}$ and Nd , $B=\text{In}$) are shown in the Figures 3.4 The figure shows that the highest Seebeck coefficient for the PrIn_3 and NdIn_3 in spin calculations in the p-type region $50.68 \mu\text{V}/\text{K}$ and $52.10 \mu\text{V}/\text{K}$, respectively as shown in Figures 3.4 In the n-type region maximum value of Seebeck Coefficient for the same order of compound under study are $-53.79 \mu\text{V}/\text{K}$, $-34.54 \mu\text{V}/\text{K}$ respectively. All the calculations are carried out at 500 K temperature. From the figure it is clear for all the compounds under study the maximum value of Seebeck coefficient for n-type and p-type region at the chemical potential of 0.02 eV to -0.02 eV.



Figures 3.4 The Seebeck coefficient of PrIn₃ and NdIn₃

3.5 Electrical Conductivity

Electrical conductivity is the movement of electrical charge in a substance. Materials having large electrical conductivity will be the best thermoelectric performers. A high electrical conductivity is necessary to minimize the heating of the conductor which is produced due to the passage of electric current (Joule heating). The greatest thermoelectric materials do, however, require a lot of electrically conductive components because of their high efficiency. Charge carriers in metallic compounds are electrons, but in semiconductors, holes and electrons are in charge. The fact that the materials under test are metals makes electrical conduction by electrons easier to calculate. For a material to have thermoelectric qualities, its electronic structure is essential, and free carriers are superior conductors. Figure 3.5 illustrates the relationship between electrical conductivity and chemical potential in spin calculations for the rare-earth intermetallic AB₃, where A=Pr and Nd, B=In. Electrical conductivity is expressed in these computations in units of order 10^{20} 1/Ωms. In p-type region maximum value of electrical conductivity for PrIn₃ and NdIn₃ are 2.10×10^{20} 1/Ωms and 2.43×10^{20} 1/Ωms respectively. In type minimum value of (σ/τ) for are 0.99×10^{20} 1/Ωms and 1.16×10^{20} 1/Ωms respectively.



Figures 3.5 The electrical conductivity of PrIn₃ and NdIn₃

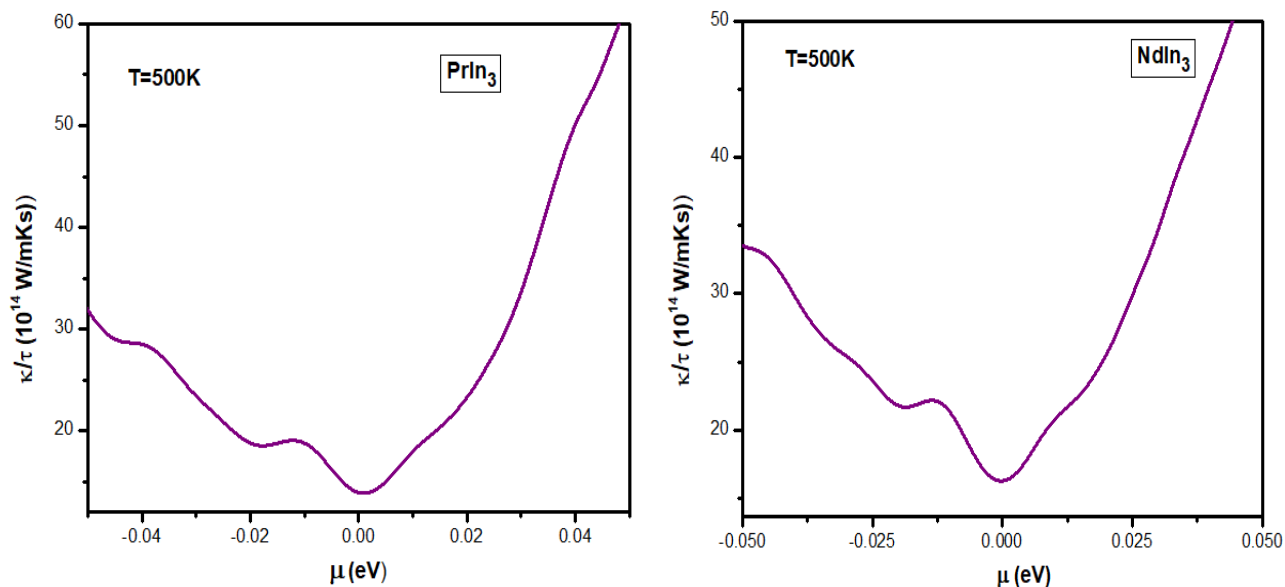
3.6 Electronic Thermal Conductivity per Relaxation Time (κ/τ)

Thermal conductivity is significantly affected by the presence of electron-hole pairs in semiconductor materials. It can be expressed as $k = k_e + k_h$, where k_e is associated with electron vibrations, and k_h corresponds to hole vibrations. In semiconductors, thermal conductivity is attributed to electron-hole pairs, while in metals, it's predominantly driven by free charge carriers or electrons. [28-31]. Thermal conductivity is the transport of heat energy through a conductor as a result of temperature gradient from the direction of high temperature to lower. In crystals, heat is conducted through free electrons and lattice vibrations. In semiconductors heat is conducted through lattice vibrations while in metals it takes place through free electrons [32]. The heat-flow measurements through the material when applying the temperature gradient are thermal conductivity. The thermal conductivity of the heat flow of the material is caused by phonemic vibrations and free electrons. The lattice part, however, contributes mainly to thermal conductivity in semiconductors, while free electrons contribute significantly to thermal conductivity in metals. The disadvantage of the BoltzTraP code is that the electronic component of thermal conductance can be determined, but thermal grid cannot be calculated. The plot of thermal conductivity per relaxation time (κ/τ) against chemical potential for AB₃ (A=Pr, Nd and B=In) at 500 K temperature are shown in Figures 3.6. From the figure it is clear that when the chemical potential increases from Fermi level i.e 0 μ (eV) on either side the (κ/τ) increases. It is realized that for the higher values of chemical potential (κ/τ) is maximum for n-type and p type region. For the compound under study the maximum value of (κ/τ) is in p-type region as compared to n-type region which show significant response of (κ/τ) in p-type region compared to n-type region. The peak value of (κ/τ) for PrIn₃ and NdIn₃ in p type region in spin calculations $28.3 \times 10^{14} \text{W/mKs}$, $22.50 \times 10^{14} \text{W/mKs}$ and in n-type are $13.78 \times 10^{14} \text{W/mKs}$ and $15.78 \times 10^{14} \text{W/mKs}$, respectively.

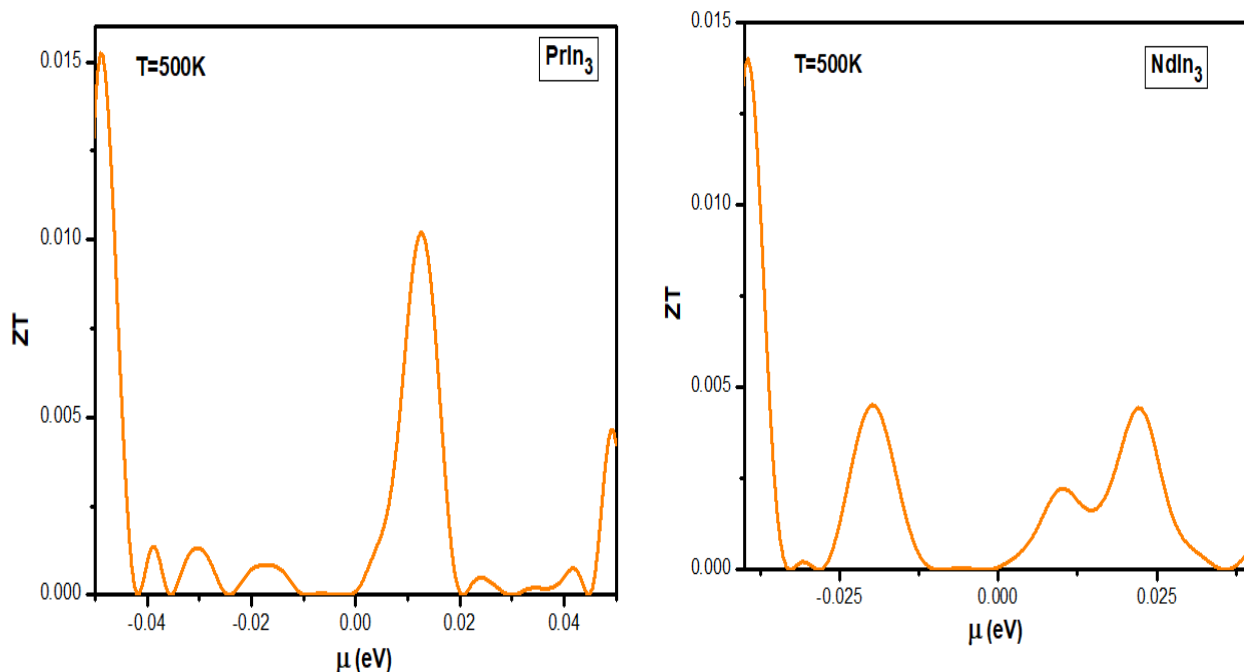
3.7 Figure of Merit

A parameter called the figure of merit is used to gauge a material's thermoelectric efficiency. The efficiency of the thermoelectric effect will increase with the merit Figure. The theoretical framework that is connected to the high Seebeck coefficient specifies the theoretical boundary of surveying the yield of thermoelectric materials. A material's ZT is an important boundary to understand a compound's productivity. Numerically it is represented as $ZT = S^2 \sigma T / \kappa$, where S, σ , κ and T are those parameters which is explain in terms of Seebeck coefficient, electrical conductivity, thermal conductivity and the temperature and also counts the

performance of the given thermoelectric boundaries [33]. High-value ZT materials are needed for industrial applications. ZT values greater than unity is known to be incredibly powerful for thermoelectric applications. Despite the fact that thermoelectric research has increased recently, scientists are still having trouble coming up with materials that may take the place of the methods used to generate energy today [34,35,36]. Figure 3.6 shows the curve of ZT against chemical potential for the rare-earth AB₃ (A=Pr, Nd and B=In) at 500K temperature. The peak ZT value for each of the compounds under study PrIn₃ and NdIn₃ is depicted as being close to the Fermi level in the picture. This means that n-type doping is a better option for materials with superior thermoelectric capabilities than p-type doping. PrIn₃ and NdIn₃ each have a peak ZT value in the figure of 0.016 and 0.014 respectively. We can see that the highest value of figure of merit is 0.016 for PrIn₃.



Figures 3.6 The thermal conductivity of PrIn₃ and NdIn₃



Figures 3.7 The thermal conductivity per relaxation time of PrIn₃ and NdIn₃

4 Conclusion

The optimized lattice parameters are obtained using generalized gradient approximation based on density functional theory. The self-consistent calculation is performed with B3PW91 hybrid functional implemented on WIEN2K package to generate the band structure and density of states for these materials. From the band structure it is observed that the valence band and conduction band overlap at the Fermi level, which shows the metallic nature of these compounds. The TDOS and partial density of state plots are also observed. The maximum contribution in TDOS is due to 4f state while other states have negligible contributions. The electronic charge density in 100 planes indicate these compounds have stronger ionic bond. The BoltzTraP code is link with the WEIN2K code to determine the thermoelectric properties. PrIn₃ has highest Seebeck coefficient value, 50.68 $\mu\text{V}/\text{K}$ among these compounds. The peak value of electronic thermal conductivity per relaxation time of NdIn₃ is 22.50×10^{14} W/mKs among these compounds.

5 Copyright Notice

This article is published by the Authors under a Creative Commons CC-BY 4.0 license. The Authors retain full copyright, with the first publication right granted to the London Journal of Physics.

References

- [1] K. N. R. Taylor, "Intermetallic rare-earth compounds," *Advances in Physics*, vol. 20, no. 87, pp. 551-660, 1971.
- [2] J. A. Abraham, G. Pagare, and S. P. Sanyal, "Ab-initio Calculations of Structural, Electronic Elastic and Mechanical Properties of REIn₃ and RETl₃ (RE= Yb & Lu) Intermetallic Compounds," *Advanced in Physics Theories and Applications*, vol. 45, pp. 66-71, 2015.
- [3] K. Purcell, D. Graf, and T. Ebihara, "High Pressure Transport Studies of NdIn₃," *APS March Meeting Abstracts*, vol. 2015, pp. G29-004, Mar. 2015.

- [4] F. Birch, "Finite elastic strain of cubic crystals," *Physical Review*, vol. 71, no. 11, pp. 809, June 1947.
- [5] P. Lethuillier, J. Pierre, K. Knorr, and W. Drexel, "Crystal fields and magnetic properties of NdSn₃, NdPb₃ and NdIn₃," *Journal de Physique*, vol. 36, no. 4, pp. 329-333, Apr. 1975.
- [6] A. M. Van Diepen, R. S. Craig, and W. E. Wallage, "Crystal field and magnetic heat capacity in PrIn₃ and CeIn₃," *Journal of Physics and Chemistry of Solids*, vol. 32, no. 8, pp. 1867-1872, Aug. 1971.
- [7] K. Satoh, Y. Fujimaki, I. Umehara, J. Itoh, Y. Ōnuki, and M. Kasaya, "Low-temperature specific heat of RIn₃ (R= La-Ho)," *Physica B: Condensed Matter*, vol. 186-188, pp. 658-660, Sep. 1993.
- [8] M. U. Salma and M. A. Rahman, "Study of structural, elastic, electronic, mechanical, optical and thermodynamic properties of NdPb₃ intermetallic compound: DFT based calculations," *Computational Condensed Matter*, vol. 15, pp. 42-47, Feb. 2018.
- [9] M. Shafiq, M. Yazdani- Kachoei, S. Jalali-Asadabadi, and I. Ahmad, "Electric field gradient analysis of RIn₃ and RSn₃ compounds (R= La, Ce, Pr and Nd)," *Intermetallics*, vol. 91, pp. 95-99, Nov. 2017.
- [10] J. P. Sanchez, J. M. Friedt, G. K. Shenoy, A. Percheron, and J. C. Achard, "Electronic and magnetic properties of rare-earth-Sn₃ compounds from 119Sn Mossbauer spectroscopy," *Journal of Physics C: Solid State Phys*, vol. 9, no. 11, pp. 2207-2218, Jun. 1976.
- [11] I. Umehara, N. Nagai, and Y. Ōnuki, "de Haas-van Alphen effect in PrIn₃," *Journal of the Physical Society of Japan*, vol. 60, no. 9, pp. 3150-3153, Sep. 1991.
- [12] I. Umehara, T. Ebihara, N. Nagai, K. Satoh, and Y. Fujimaki, "Magnetoresistance and de Haas-van Alphen effect in the antiferromagnetic compound NdIn₃," *Journal of the Physical Society of Japan*, vol. 61, no. 5, pp. 1633-1644, May 1992.
- [13] K. Satoh, Y. Fujimaki, I. Umehara, J. Itoh, Y. Ōnuki, and M. Kasaya, "Low-temperature specific heat of RIn₃ (R= La-Ho)," *Physica B: Condensed Matter*, vol. 186, pp. 658-660, Jan.1993.
- [14] T. Ebihara, I. Umehara, A. K. Albessard, K. Satoh, and Y. Ōnuki, "Fermi surface property of branch d in CeIn₃," *Physica B: Condensed Matter*, vol. 186, pp. 123-125, Jan. 1993.
- [15] C. Fiolhais, F. Nogueira, and M. A. Marques, Eds., *A Primer in Density Functional Theory*, vol. 620. Springer Science & Business Media, 2003. [ISBN: 3-540-03082-2]
- [16] K. Burke, "Perspective on density functional theory," *The Journal of Chemical Physics*, vol. 136, no. 15, p. 150901, 2012.
- [17] E. Fabiano, L. A. Constantin, and F. D. Sala, "Exchange-correlation generalized gradient approximation for gold nanostructures," *The Journal of Chemical Physics*, vol. 134, no. 19, pp. 194112-194121, 2011.
- [18] Morrison, R. A. (2019). Equations of State, Sound Velocities, and Thermo-elasticity of Iron-Nickel-Silicon Alloys in the Earth's Inner Core (Doctoral dissertation, California Institute of Technology).
- [19] A. Gerolin, J. Grossi, and P. Gori-Giorgi, "Kinetic correlation functional from the entropic regularization of the strictly correlated electrons problem," *Journal of Chemical Theory and Computation*, vol. 16, no. 1, pp. 488-498, 2019.
- [20] P. Blaha, K. Schwarz, G. Madsen, D. Kvasnicka, and J. Luitz, "WIEN2k, An augmented plane wave plus local orbitals program for calculating crystal properties user's guide," 14.2, Vienna University of Technology, Inst. Physical & Theoretical Chem., Getreidemarkt 9/156, A-1060 Vienna, Austria, 2014.
- [21] Witt, W. C., Shires, B. W., Tan, C. W., Jankowski, W. J., & Pickard, C. J. (2021). Random Structure Searching with Orbital-Free Density Functional Theory. *The Journal of Physical Chemistry A*, 125(7), 1650-1660.
- [22] K. Schwarz and P. Blaha, "Solid state calculations using WIEN2K," *Computational Material Science*, vol. 28, no. 2, pp. 259-273, 2003.

- [23] C. E. Ekuma, D. J. Singh, J. Moreno, and M. Jarrell, "Optical properties of PbTe and PbSe," *Physical Review B*, vol. 85, no. 8, pp. 85205-85213, 2012.
- [24] Ali Z, Khan I, Rahman M, Ahmad R and Ahmad I. Electronic structure of the LiAA' O 6 (A= Nb, Ta, and A'= W, Mo) ceramics by modified Becke-Johnson potential. *Opt. Mater.* 2016, 58: 466.
- [25] Ali Z, Shafiq M, Asadabadi SJ, Aliabad HR, Khan I and Ahmad I. Magneto-electronic studies of antiperovskites NiNMn₃ and ZnNMn₃. *Comput. Mater. Sci.* 2014, 81: 141.
- [26] Wang Z, Moosavi SH, Kroener M and Woias P. Development of a Thermoelectric Nanowire Characterization Platform (TNCP) for Structural and Thermoelectric Investigation of Single Nanowires. Thermoelectric Bi₂Te₃ Nanomaterials. 2015.
- [27] Aliabad HR, Ghazanfari M, Ahmad I and Saeed M. Ab initio calculations of structural, optical and thermoelectric properties for CoSb₃ and ACo₄Sb₁₂ (A= La, Tl and Y) compounds. *Comput. Mater. Sci.* 2012, 65: 509.
- [28] J. N. Hausmann, M. Oudah, A. Ikeda, S. Yonezawa, and Y. Maeno, "Controlled synthesis of the antiperovskite oxide superconductor Sr_{3-x}SnO," *Superconductor Science and Technology*, vol. 31, no. 5, pp. 055012-055018, 2018..
- [29] X. Yuan et al., "Design of negative/nearly zero thermal expansion behavior over a wide temperature range by multiphase composite," *Materials & Design*, vol. 203, pp. 109591-109601, 2021
- [30] H. Yamamoto, T. Imai, Y. Sakai, and M. Azuma, "Colossal negative thermal expansion in electron-doped ABX tetragonal," *Angewandte Chemie International Edition*, vol. 57, no. 27, pp. 8170-8173, 2018.
- [31] Janesko, B. G., Verma, P., Scalmani, G., Frisch, M. J., &Truhlar, D. G. (2020). M11plus, a range-separated hybrid meta functional incorporating nonlocal rung-3.5 correlation, exhibits broad accuracy on diverse databases. *The journal of physical chemistry letters*, 11(8), 3045- 3050.
- [32] Rabin, Y.-M. Lin, and M. S. Dresselhaus, "Anomalously high thermoelectric figure of merit in Bi_{1-x}Sb_x nanowires by carrier pocket alignment," *Applied Physics Letters*, vol. 79, no. 1, p. 81, 2001
- [33] Feng Y., Zhang J., Qin P., Liu, S., Yang, Q., Meng, J. &Xie, J. (2019). Characterization of elevated-temperature high strength and decent thermal conductivity extruded Mg-Er-Y-Zn alloy containing Nano-spaced stacking faults. *Materials Characterization*, 155, 109823- 109834.
- [34] A. H. Sofi and M. A. Shah, "Structural and electrical properties of copper doped In₂O₃ nanostructures prepared by citrate gel processes," *Materials Research Express*, vol. 6, no. 4, pp. 45039-45047, 2019.
- [35] H. Hardianto, "Textile-Based Thermoelectric Generators Based on Conductive Yarns," Doctoral dissertation, Ghent University, 2020
- [36] K. A. Moltved and K. P. Kepp, "The Metal Hydride Problem of Computational Chemistry: Origins and Consequences," *The Journal of Physical Chemistry A*, vol. 123, no. 13, pp. 2888-2900, 2019.